Temperature effects on the elastic properties of hysteretic elastic media: Modeling and simulations

M. Nobili* and M. Scalerandi†
INFM—Dip. Fisica, Politecnico di Torino, C.so Duca degli Abruzzi 24, 10129 Torino, Italy
(Received 19 September 2003; revised manuscript received 19 December 2003; published 17 March 2004)

Different materials with mesoscopic characteristics (e.g., defects or intergrain regions) have been shown to share a peculiar elastic behavior when subject to temperature variations. We present here a simple model based on the description of the mesoscopic features as bistate bond regions that connect elastic portions described by the traditional Landau thermoelastic theory. We apply our model to simulate resonance frequency experiments in order to analyze the effects of temperature changes on the elastic properties of materials and reproduce part of the phenomenology observed concerning the conditioning effect and the recovery of the system to its original state after a thermal shock.

DOI: 10.1103/PhysRevB.69.104105 PACS number(s): 62.30.+d, 91.60.−x, 02.70.−c

I. INTRODUCTION

In recent years, several anomalous elastic effects due to mechanical stresses have been shown for a wide variety of materials: rocks, sandstones, concrete, structural materials with mesoscopic flaws, etc.[1] Among them, quasistatic experiments have revealed the existence of a hysteretic loop in the stress-strain relation with end-point memory,[2] while, through dynamic experiments, phase shifts in resonance experiments,[3] the generation of higher-order harmonics[1] and sidebands[4] with a well-defined rate, nonclassical attenuation,[5] and other effects have also been found. Perhaps the most striking feature observed so far is the so-called ''slow dynamics'', which consists of a downshift in the resonance frequency when the specimen has been dynamically excited and consequent recovery proportional to the logarithm of the elapsed time.[6,7]

A complete understanding of the basic properties and behavior of such materials is still missing and requires both molecular dynamics[8] and numerical simulations at the mesoscopic level.[9] Nevertheless, several phenomenological models have been proposed in the last years and have been proven to be capable to reproduce the observed phenomenology. For instance, the interactions between elastic waves and cracks have been recently described using the Luxemburg-Gorky effect,[10] and quasistatic stress-strain loops can be well reproduced using a Preisach-Mayergoyz (PM) representation.[11–13] Also dynamic experiments can be modeled using pseudopotential approaches.[14]

Based on a spring model approach,[15,16] we have recently proposed a description of such hysteretic materials as linearly elastic portions (grains) separated by bond regions (interstices). The latter may be in either of two different elastic states, according to the current and previous applied stresses. Our model has allowed us to describe, with the same approach, most of the observed phenomenology both in quasistatic[17,18] and dynamic experiments.[19] In addition, using thermal random transitions among the two states, our model has allowed us to simulate also the slow dynamics, in excellent agreement with the observed log time recovery.[18,20]

Nevertheless, most of the work, both experimental and theoretical, performed until now has been devoted to the description of effects related to mechanically induced strains, both through elastic wave generators[3,5] or impacts.[21] Also, water saturation effects have been extensively studied from an experimental point of view.[22,23] In more recent years, interest has been devoted to analyze the anomalous elastic behavior of hysteretic materials induced by temperature changes. Results suggesting hysteretic loops have been found for the resonance frequency versus temperature curves,[24] which reveal an anomalous softening occurring during material cooling. More results[25] show that temperature changes (in most cases both cooling and heating), besides inducing softening, also cause a conditioning of the material, which slowly (and logarithmically) disappears (recovery).[26,7] All of this results concur to sustain the hypotheses that slow dynamics may also be caused by thermal shocks, in addition to the widely discussed slow dynamics impact induced.[7]

In the present contribution, we show that the model we have previously presented[19,20] allows us to reproduce most of the temperature-induced phenomenological observations, once classical linear thermoelastic effects[27] are included in the description of the grain portions. Without any modification to the description of the nonlinear protocol used to define the elastic properties of interstices, we describe here both the anomalous resonance frequency shifts and its recovery. In addition, our model allows us to give an easy interpretation of the observed data and to predict further observations that may be obtained with proper experiments.

In the first section, the model, as described in detail in Ref. 20, will be very briefly reviewed, with the addition of terms that keep account of the stress-temperature coupling. In the following section, numerical results concerning both the variation of the elastic constants with temperature and the conditioning and slow dynamics caused by thermal shocks will be analyzed. Finally, in the Conclusion, we will highlight further perspectives and a few preliminary results we are currently obtaining.

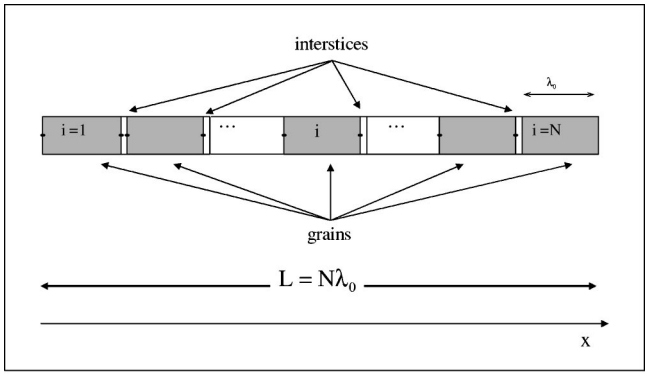

FIG. 1. Schematic representation of a 1D bar of hysteretic material. Grains (linear) are separated by much shorter interstices (hysteretic).

II. THE MODEL

Let us consider a multigrained material specimen. If it consists of a thin bar, as is the case in most experimental setups, we can simplify the problem with a one-dimensional (1D) model, in which grains alternate with interstices. Grain portions are much larger than interstices, of the order of 10–20 μm versus 1 μm. For simplicity, we will assume that at equilibrium (i.e., in the absence of external forces and at some given temperature T_0) all grains have the same rest length λ_0, the same elastic constant K, and the same mass $m=\rho\lambda_0$, where ρ is the density. We consider as negligible both the interstice rest length δ_0 and its mass.

The full specimen, of length $L=N\lambda_0$, consists of N grains (labeled with integer numbers $i=1,...,N$) and $N-1$ interstices (see Fig. 1). Its elastic behavior under an external perturbation $F(t)$, i.e., when the length of each grain and each interstice [$\lambda_i(t)$ and $\delta_i(t)$, respectively] are time dependent, can be determined once the equation of state for both grains and interstices are given, as discussed in the next subsections (for more details see Ref. 20). Note that in the following the index i will be omitted for simplicity for all quantities except when they are firstly defined.

A. Single-grain constitutive equations

Based on experimental observations, we assume the hysteretic nonlinearity to be confined to the interstice region. Therefore grains follow the usual thermoelastic theory.[27] The constitutive equations, i.e., the relation between stress $\sigma_i(t)$ and strain $\varepsilon_i(t)=[\lambda_i(t)-\lambda_0]/\lambda_0$, at a given temperature T_i for the ith grain, neglecting classical nonlinear terms, are given as

$$\sigma(t)=K\varepsilon(t)-K\alpha(T-T_0), \tag{1}$$

where α is the thermal expansion coefficient of the specimen. Note that in Eq. (1) we have assumed that the Young and bulk moduli are approximately equivalent. If the body is at a temperature different from the equilibrium temperature (T_0), then, even if there are no external forces, grains are deformed with consequent generation of internal stresses, which disappears when a new equilibrium, corresponding to the new temperature, is reached.

In addition to Eq. (1), the state of the grain is determined by the 1D thermal conduction equation

$$C\frac{\partial T}{\partial t}=k\frac{\partial^2 T}{\partial x^2}-\alpha KT\frac{\partial}{\partial t}\frac{\partial \varepsilon}{\partial x}, \tag{2}$$

where k is the thermal conductivity and C is the specific heat. Finally, the elastic constants of a solid are temperature dependent. In most cases, the medium becomes stiffer with decreasing temperature according to the following law:[28]

$$K(T)=a-\frac{bT^2}{T+c}, \tag{3}$$

where a, b, and c are constants.

B. Single-interstice constitutive equations

The constitutive equation for interstices should keep account of nonlinear effects. As a consequence, the stress $\tau_i(t)$ on the ith interstice has, in general, a complex dependence on external factors, such as the pressure

$$\begin{aligned} P_i(t)&=\sigma_{i+1}(t)-\sigma_i(t)\\ &=K[\varepsilon_{i+1}(t)-\varepsilon_i(t)]-K\alpha(T_{i+1}-T_i), \end{aligned} \tag{4}$$

the interstice strain $\eta_i(t)=(\delta_i(t)-\delta_0)/\delta_0$ and its time derivatives, the temperature difference between the interstice tips ΔT_i, etc.:

$$\tau(t)=f(P(t),\eta(t),\dot{\eta}(t),\Delta T). \tag{5}$$

The explicit equation should be evinced from a detailed knowledge of interaction mechanisms at the molecular or mesoscopic level, e.g., dislocation theory,[29] Biot theory for capillary pressure,[30] glass transitions,[31] etc. However, since such information is not yet available, in previous papers we have shown that the choice of a phenomenological ''two-state'' constitutive equation allows us to reproduce most of the observations obtained in both dynamic[19,20] and quasistatic experiments[17,18] at constant temperature.

We assume that the interstice may be in one of the following linear states, being nonlinear only due to sudden transitions from one state to the other (as will be discussed later):

State A: The interstice is rigid. Any disturbance is propagated across the interstice without straining it. The existence of a rigid interstice state is motivated by the experimental observation of residual strains at $P=0$ in quasistatic compressional experiments.[2,18] In fact, residual strains at zero stress, which disappear very slowly with time, imply the (at least temporary) existence of interstice configurations, reached during phases of increasing pressure, which remain ''frozen'' during pressure release.

State B: This is a linear elastic state, in which

$$\tau(t)=a_1P(t)+a_2\eta(t)+a_3\dot{\eta}(t)+a_4\Delta T, \tag{6}$$

where the parameters a_n $(n=1,2,3,4)$ are constant. More complex states may be of course modeled using higher-order expansions for the stress τ. However, as already mentioned,

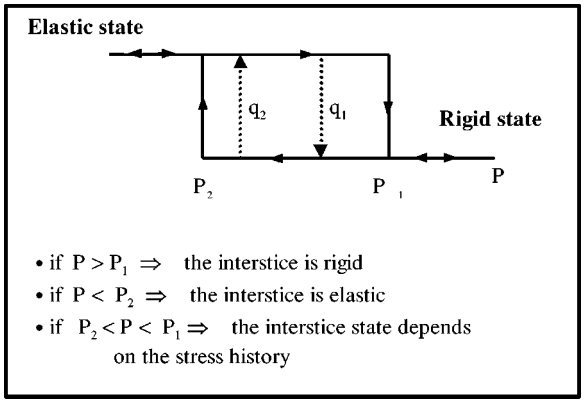

FIG. 2. Basic hysteretic loop for each hysteretic mesoscopic unit (HMU). q_1 and q_2 are the thermal activated transition rates between the two states.

previous studies[19] have shown that the first order expansion given by Eq. (6) is sufficient to reproduce completely the observed phenomenology.

Furthermore, we assume that the temperature is uniform along the interstice. Hence $\Delta T=0$. Such an assumption is only a reasonable (due to the short length of the interstice and the 1D treatment adopted) first approximation. In our opinion, including local high-temperature gradients (such as those observed in the Gorky-Luxembourg effect) will only contribute to reinforce the agreement of the model results with the experimental findings. In addition, an explicit thermoelastic equation [similar to Eq. (2)] for the interstice itself may help to catch additional experimentally observed features and, perhaps, enable us to explain the physical origin of the phenomenological equation of state adopted here (work in progress).

As already mentioned, nonlinearity and hysteresis emerge once the rules for the transition from the rigid to the elastic state (and vice versa) are defined. For this purpose (see Fig. 2), we define for each interstice a pair of parameters (P_{1_i},P_{2_i}) and we assume that the interstice is in the rigid state if $P>P_1$ or in the elastic state if $P<P_2$. In the intermediate-pressure range $(P_2<P<P_1)$ the two states coexist and the interstice is in one state or the other depending on the previous stress history. In fact, the protocol is defined as follows. Starting for any given interstice at a given pressure $P<P_1$, we assume that the interstice length varies elastically up to $P=P_1$, at which point it becomes rigid. Conversely, when P decreases, the interstice remains rigid up to the value $P=P_2$, where it becomes elastic again.

In addition to such hysteretic behavior, Fig. 2 shows thermally activated random transition (with rates q_1 and q_2) between the two linear states in the pressure range in which they coexist. Since the rigid state seems to us to be more stable than the elastic state (the rigid-elastic transition implies the rupture of a sort of ''static bond''), we assume for the thermal activated transition rates that $q_1>q_2$. These hopping transition rates increase, of course, with the temperature, but in the present context, this dependence is not explicitly included. Likewise, any other dependence of the rates on, e.g., the applied pressure P and/or the difference $(P-P_{1,2})$, is neglected.

C. Equations of motion

From the constitutive laws, the equations of motion can be easily obtained using Newton's law. By defining

$$u_i^+=\sum_{j\leqslant i}[\lambda_j(t)+\delta_j(t)],$$

$$u_i^-=\lambda_i(t)+\sum_{j<i}[\lambda_j(t)+\delta_j(t)], \tag{7}$$

the positions of the right and left tips of the ith interstice are

$$\frac{m}{2}\ddot{u}_i^-=\sigma_i+\tau_i-\gamma\dot{u}_i^-,$$

$$\frac{m}{2}\ddot{u}_i^+=\sigma_{i+1}-\tau_i-\gamma\dot{u}_i^+, \tag{8}$$

where dots denote time derivatives and an attenuative term with coefficient γ has been included.

It follows that

$$\frac{m\lambda_0}{2}\ddot{\varepsilon}_i=\frac{m}{2}(\ddot{u}_i^--\ddot{u}_{i-1}^+)=\tau_i+\tau_{i-1}-\gamma\lambda_0\dot{\varepsilon}_i \tag{9}$$

and

$$\frac{m\delta_0}{2}\ddot{\eta}_i=\frac{m}{2}(\ddot{u}_i^+-\ddot{u}_i^-)=\sigma_{i+1}-2\tau_i-\sigma_i-\gamma\delta_0\dot{\eta},$$

elastic state,

$$\ddot{\eta}_i=\dot{\eta}_i=0, \quad \text{rigid state}, \tag{10}$$

where the choice of equation of motion for the interstice strain depends on the interstice state.

Note that, according to Eq. (10), the rigid state can be described by the same equation of state as the elastic one [Eq. (6)] with $a_1=0.5$ and $a_2=0$. Furthermore, the elastic to rigid transition causes a discontinuity in $\dot{\eta}_i$ (being $\dot{\eta}_i\neq 0$ in the elastic state). Hence, imposing the sudden transition to $\ddot{\eta}_i=0$, we also obtain $a_3=(\sqrt{K/\rho}/4.0+\gamma/2.0)\delta_0$, which becomes irrelevant once in the rigid state.

Using Eqs. (1), (2) and (6), iteration equations can be easily obtained by means of the usual finite difference (FD) formalism for the time derivatives. These iteration equations are omitted here for brevity, but are reported in Ref. 20.

D. Initial and boundary conditions

We assume that at the beginning (i.e., before starting the ''virtual experiment'') the specimen is completely relaxed (i.e., a long time, usually overnight in real experiments, has passed since the last perturbation of the specimen, either thermal or mechanical) and kept at atmospheric pressure P_0 and room temperature T_0. For simplicity we redefine the pressure scale, so that $P_0=0$. Three cases are possible (see Fig. 2):

$P_2>0$: The interstice is in the elastic state.

$P_1<0$: The interstice is in the rigid state.

$P_2<0<P_1$: Both states are allowed. Since the specimen is relaxed, the state distribution is in equilibrium condition. Hence their respective probabilities are given by

$$p(\text{elastic}) = 1 - p(\text{rigid}) = \frac{q_2}{q_1 + q_2}. \tag{11}$$

In a dynamics experiment, the boundary conditions are given by an external forcing at one end of the bar [e.g., the displacement is given by $u_1(t) = u_0 \cos(\omega t)$ for a monochromatic wave] and free boundary conditions (zero stress) at the other. The temperature at the two tips of the bar is controlled and kept at a value T_{ext}.

The choice of the pair of pressures (P_1, P_2) for each interstice is, of course, crucial. Such a set is usually represented in the so-called Preisach-Mayergoyz (PM) space, i.e., as a distribution of points in a (P_1, P_2) plane, which, in the case of virtual quasistatic experiments, is obtained by inverting the experimental data.[17,18] For the simulation of resonant dynamic experiments the range of pressures is usually much smaller and only an extremely small portion of the PM space around the ambient pressure P_0 is explored by the incoming perturbation. In such a tiny region, it is reasonable to assume a uniform distribution of (P_1, P_2) points, which is approximately (due to the limited number of units) done in our simulations.

III. RESULTS AND DISCUSSION

In this section, we consider the problem of the determination of the resonance frequencies of a 1D bar, i.e., of its elastic properties. We assume that a rod-shaped specimen is equipped with a transducer generating monochromatic waves of excitation amplitude A attached at one end and with an accelerometer attached to the other end. The frequency $f = \omega/2\pi$ is swept through one resonance mode f_r of the specimen (we will present results here for the third resonance mode) and the time-averaged acceleration amplitude A_r (in stationary conditions) is recorded. This procedure of resonance curve tracking is repeated at different temperatures (experiment type A) and/or after different thermal shocks (experiment type B). The description of the two experiments is reported in Fig. 3, where the behavior of the external temperature is reported versus time. Both heating and cooling (negative ΔT) have been examined and the behavior of the resonance frequency has been followed in time. Resonance frequencies are always measured at thermal equilibrium, i.e., the resonance frequency is not tracked during the heating or cooling processes. In particular, in both experiments measurements are performed at time t_a (on a specimen fully relaxed, i.e., in complete equilibrium, and before the thermal change), t_b (immediately after the thermal change, i.e., without relaxation but in thermal equilibrium), and tracked from t_b to t_c.

A. Parameters

The values of parameters used in the simulations have been chosen in a range valid for rock samples used in most

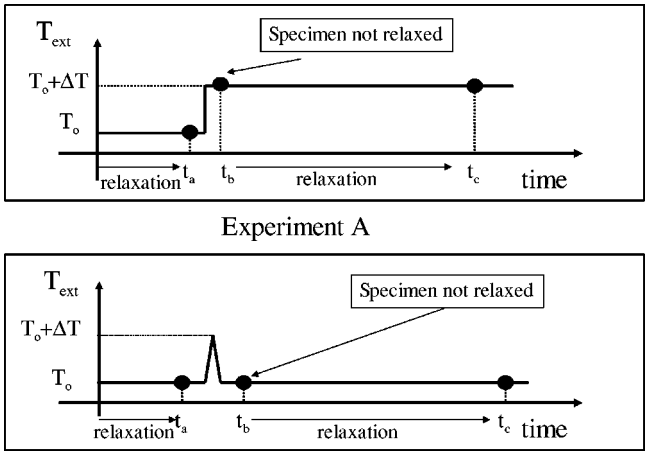

FIG. 3. Behavior of the temperature vs time for the two kind of virtual experiments performed. In both cases, at time t_a and t_c complete relaxation of the system to an equilibrium state is obtained. At time t_b, complete thermal equilibrium is reached, but not relaxation. Note that the time scales in the plot are only indicative: thermal equilibrium (t_a to t_b) is reached in milliseconds, while mechanical equilibrium (before t_a and from t_b to t_c) needs a few hours.

of the experiments (see, e.g., Ref. 32). Typically, the wave velocity ranges between $v = 1800$ and $v = 2600$ m/sec, densities are about 2000–3000 kg/m^3 and the linear attenuation parameter Q varies from 10 to 200. Strains used in experiments are very small but occur in a wide range (of the order of 10^{-8}–10^{-6}).

Unless otherwise specified, we have chosen a bar with typical dimensions used in neutron scattering experiments:[33] length $L = 21$ mm and cross section of about $S = 10$ mm^2 (which is not relevant for the simulations). Using longer specimens is of course more time consuming but computationally affordable up to a length of 20–40 cm. Grain and interstice typical lengths are chosen as $\lambda_0 = 20\ \mu$m and $\delta_0 = 1\ \mu$m. It follows that $N = 1000$. The specimen elastic constant and densities are $K = -10$ GPa and $\rho = 2300$ kg/m^3 (typical values for Berea sandstone). Furthermore, in absence of available experimental data, we assume arbitrarily for the interstices $a_1 = 0.95$ GPa, $a_2 = 28.5$ GPa, and $a_3 = 50$ GPa sec. We note that we have verified that the qualitative behavior of the system does not depend on the choice of such parameters. Also, $q_1 = 1.5 \times 10^{-11}$, $q_2 = 0.03 q_1$, and P_1 and P_2 ranges in the pressure interval $[-1.0, 1.0]$ MPa, which is smaller than (but of the same order of magnitude as) the yield modulus. It follows that the expected fundamental resonance frequency of the bar (neglecting the interstice contribution) is about 25 kHz (and the third mode, used in the simulations, is at about 0.125 MHz). Considering as a linear case the situation in which interstices contribute to the elastic constants but are permanently in the initial condition state (i.e., no switch occurs), we expect a linear (i.e., in the limit of strain going to zero) third mode resonance frequency slightly smaller than 0.125 MHz.

The other parameters chosen are a room temperature of $T_0 = 300$ K, thermal expansion coefficient $\alpha = 2.2 \times 10^{-7}$ K^{-1}, thermal diffusion coefficient $k = 3.2$ kg m/K

$\sec^3$, heat capacity $C=0.32$ J/m^3 K, and viscosity $\gamma=37.5$ kg/m^2 s. The estimated (from a linear approximation) Q factor is 22 (Q is the resonance frequency/bandwidth of the resonance curve in the limit of zero injection amplitude[34]).

Finally, the parameters in Eq. (3) have been chosen $a=11.3$ GPa, $b=7$ MPa/K and $c=100$ K. The forcing amplitude is chosen to be very small, to correspond to a strain ($\zeta_{inp}\sim u_0 2\pi\omega/v$) of the order of 6×10^{-8} (which, in resonance, due to the interference of multiple reflections, becomes 10 times larger: $\zeta_{\rm res}=10\zeta_{inp}=6\times10^{-7}$). Therefore, the forcing amplitude corresponds to a force $F_0=SK\zeta_{inp}=6$ mN (from now on we will use F_0 to characterize the amplitude of the forcing rather than u_0).

Given the choice of parameters, it follows that the time scales in the experiments correspond well to those experimentally observed (note that time scales in Fig. 3 are purely indicative). In fact, standing-wave conditions are reached in tens of milliseconds (in agreement with the estimate obtained from the ratio $5Q/f$, considering that Q is smaller than its linear approximation due to a nonlinear contribution to attenuation), a frequency sweep is performed in about 1 min, thermal equilibrium (i.e., the time interval from t_a to t_b) is reached very fast (in about 1 msec), and relaxation (t_b to t_c) in a few hours. Note that thermal equilibrium is reached so fast in the simulations because an additional term is included in the model to simulate thermal exchange from the lateral surfaces of the specimen. This contribution, however, does not modify the values of the peak stress, which is reached at very early times in the process of relaxation to thermal equilibrium (see, e.g., Fig. 7). As a consequence, the introduction of such ''lateral thermal exchange'' is not relevant, both qualitatively and quantitatively, for the model predictions.

B. Variation of the elastic properties with temperature (experiment A)

1. Virtual experiments

Let us first consider the variation of the specimen elastic properties with temperature. To this purpose, the resonance frequency is measured at different temperatures, always in thermal equilibrium, but without letting the system relax before performing the frequency sweep: referring to Fig. 3, experiments of type A for different ΔT are performed. In Fig. 4, we plot the averaged acceleration versus frequency at time t_b for different temperatures $T_{\rm ext}$, as reported in the plot, for both a linear [Fig. 4(a)] and a nonclassical nonlinear [Fig. 4(b)] specimen. As expected, in the linear case the resonance frequency (i.e., the frequency corresponding to the peak of the resonance curve) shifts to the right (increasing frequency) with decreasing temperature. The shift is very small, but noticeable, especially in the inset of Fig. 4(a). Such an effect, due to the variation in the elastic constants described by Eq. (3) is well known and common to most materials. Attenuation is not (or at most very slightly) affected by the temperature change, as shown by the absence of any noticeable change of the curves amplitude and width.

The opposite takes place in the case of a hysteretic material [Fig. 4(b)]. Here, the resonance frequency f_r drops down

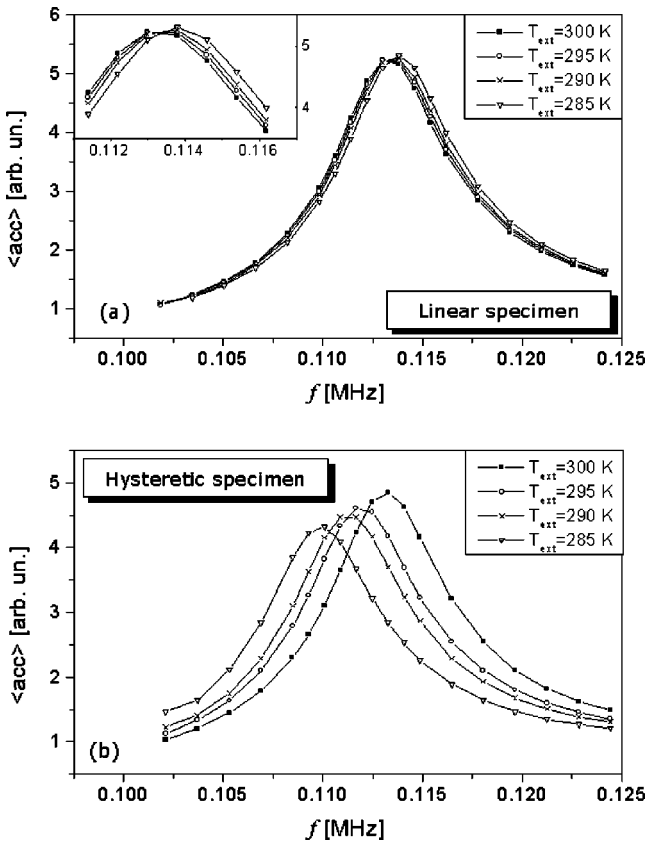

FIG. 4. Experiment type A: averaged acceleration vs frequency for different values of the external temperature. (a) linear specimen; (b) hysteretic specimen.

with decreasing temperature, indicating a softening of the specimen.[24] It is to be noted that, in agreement with experimental data,[25,7] such softening is observed both when the material is cooled and heated (not reported for brevity). Additional preliminary simulations have shown that, according to the choice of parameters, it is possible to describe cases in which, in the hysteretic case, an initial hardening (increasing f_r with decreasing $T_{\rm ext}$) is followed by softening for a further decrease in temperature.[35] Also, the resonance curves become wider with decreasing $T_{\rm ext}$ and, more evidently, the peak values decrease, indicating a stronger attenuation (nonlinear attenuation).[7]

The results described are resumed in Fig. 5, where f_r is reported versus $\Delta T=T_{\rm ext}-T_0$. The behavior in the linear case (circles) is well fitted (solid line) by

$$f_r(\Delta T)\propto\sqrt{K(T_{\rm ext})}, \tag{12}$$

where $K(T_{\rm ext})$ is given by Eq. (3). The anomalous behavior in the hysteretic case (squares) is, as noted, in agreement with experimental data. Note the slight asymmetry in the hysteretic case: the resonance frequency drops slightly more under cooling ($\Delta T<0$) than heating (for the same of value of $|\Delta T|$).

Finally, in Fig. 6 we have considered a hysteretic material and performed a recovery experiment (see Fig. 3). First we have tracked the resonance frequency versus time at $T_{\rm ext}$

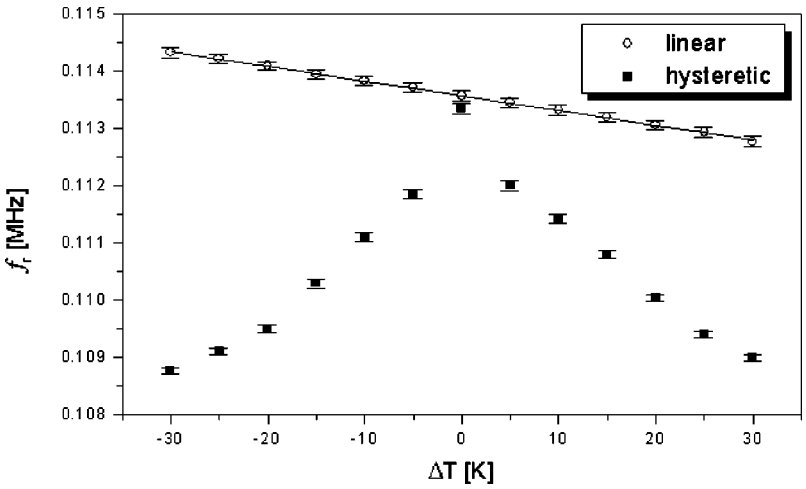

FIG. 5. Resonance frequency vs temperature variation with respect to the room temperature. Note that $\Delta T>0(<0)$ corresponds to heating (cooling).

$=T_0=300$ K for 10 min up to t_a. Starting from this initial situation ($T_0=300$ K), we have considered two cases:

Case 1: The specimen is cooled by immediately decreasing the external temperature T_{ext} by 20 K to 280 K ($<T_0$) (upper plot).

Case 2: The specimen is heated by immediately increasing the external temperature T_{ext} by 20 K to 320 K ($>T_0$) (bottom plot).

In both cases, as soon as the external temperature is changed (and after thermal equilibrium is reached), the resonance frequency drops, in agreement with that previously discussed ($t_a<t<t_b$). However, the drop is larger during cooling (an explanation of this behavior may be found in Ref. 36). Later on ($t_b<t<t_c$), relaxation occurs and the material becomes harder with a logarithmic time recovery: the resonance frequency recovers the values that would have been expected if the material was linear: harder (softer) than at $T_{\text{ext}}=T_0$ for the cooling (heating) cases (the behavior of a corresponding linear material is shown as a dashed line). The qualitative agreement with experimental data is rather good.[7]

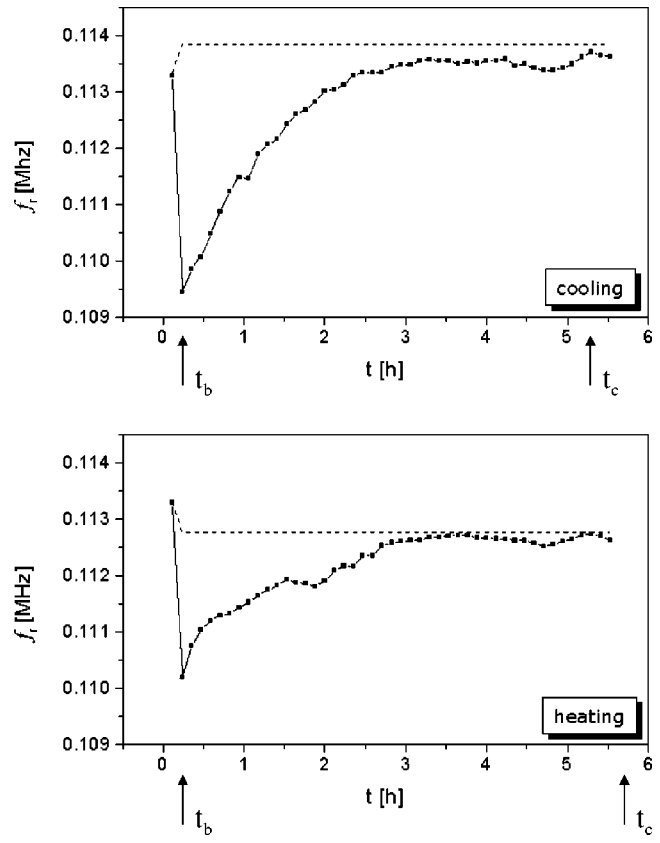

FIG. 6. Resonance frequency vs time during a type A experiment recovery. In both plots the dashed line represents the frequency behavior expected for a linear specimen.

It is to be noted again that, according to the parameter values, in some cases the initial drop (only during cooling) is replaced by an initial increase, followed by a (logarithmic with time) further increase. Such anomalous behavior (and its relation with the choice of the parameters) is currently under investigation.

2. Discussion

The anomalous behavior of hysteretic specimens presented in Figs. 4–6 can be explained as a ''competition'' between two effects. On one hand, the variation of the grain elastic constants with temperature induces a softening (hardening) with heating (cooling) of the same entity as that observed in the linear case. On the other hand, the temperature variation induces local stresses within the bar, with a consequent change of state of some interstices and relative variation of the elastic properties, shown both experimentally[6] and theoretically[20] to produce softening, independently of the stress sign (compression or tension), hence on the heating (cooling) process.

To further prove such interpretation, in Fig. 7(a) the pressure applied to a selected interstice ($i=500$) during the process of thermal conduction is reported versus time for $\Delta T=-30$ K. The local stress applied to interstices, due to the dilatation of the surrounding grains, is much larger than the stress due to the perturbing waves during the resonance curve tracking (which is of the order of $K\zeta_{\text{res}}=6$ KPa). Hence, thermally induced pressure [whose range is depicted in Fig. 7(b) as a triangle] might be sufficient to switch permanently (except for thermal relaxation) the state of some interstices from the rigid to the elastic state (or vice versa, depending of the corresponding values of P_1 and P_2).

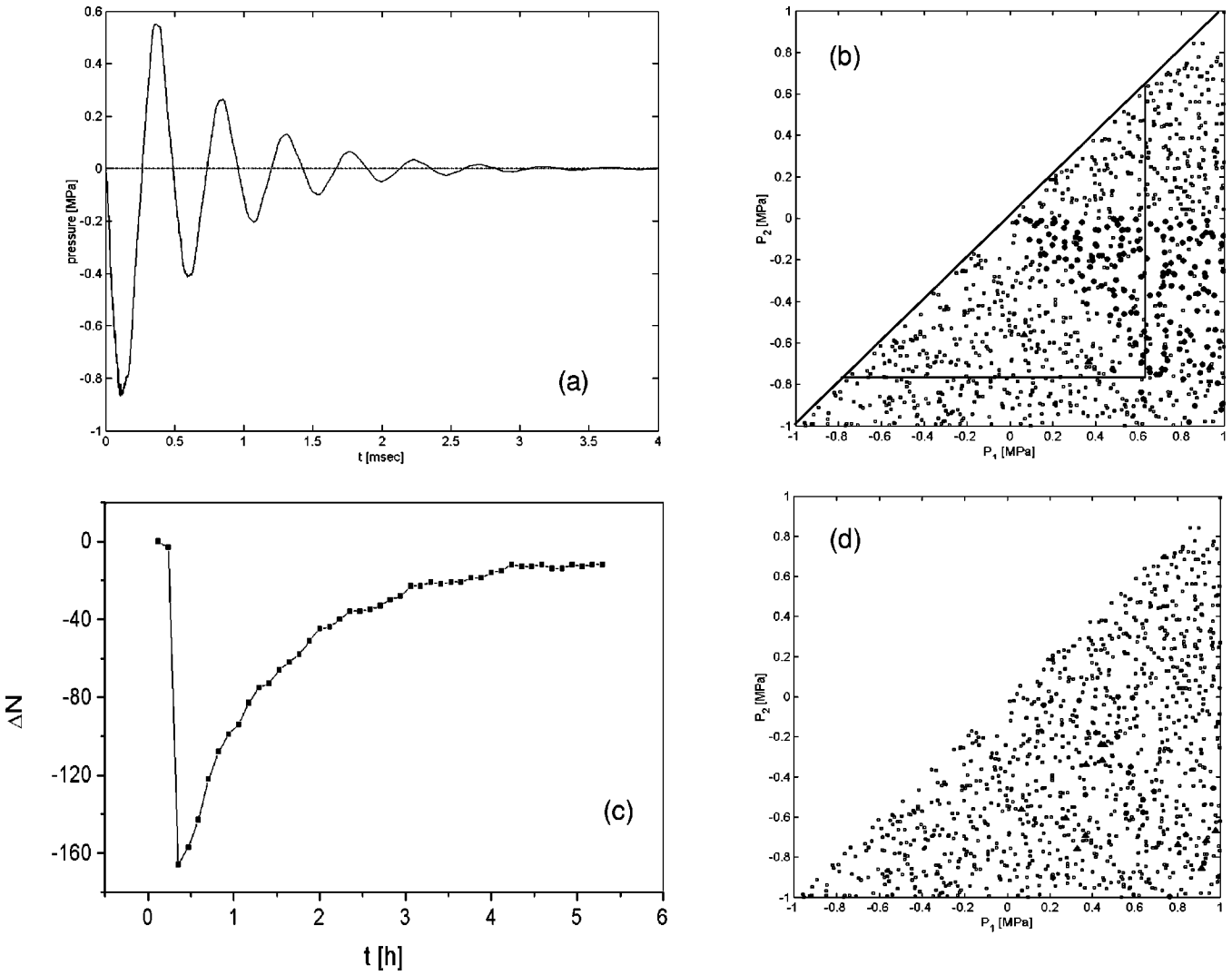

FIG. 7. Determination of the stresses induced by a temperature variation $\Delta T=-30$ K (cooling). (a) Pressure on the $i=500$ interstice vs time during thermal equilibrium assessment. (b) Distribution in the PM space after thermal equilibrium is reached. Small dots denote units that have not changed state from the initial one, triangles represent units shifted from the elatic to the rigid state, and circles denote units shifted from the rigid to the elastic state. The triangle marked in bold lines identifies the pressure range of the induced stress. (c) ΔN vs time during recovery (ΔN is the net number of interstices that have become softer due to the stress applied). (d) Distribution in the PM space when recovery is fully accomplished.

In Fig. 7(b), the distribution of the interstices in the PM space after the variation in temperature is reported (just before t_b in Fig. 3). Circles denote interstices switched from the rigid to the elastic state, triangles vice versa, and dots units that have not changed their state. The figure shows the dominance of the softening events, which results in a reduction of the resonance frequency [which has to be summed with the increase due to the cooling effect on the grain elastic constants: Eq. (3)]. As a result, the behaviors observed in Figs. 4 and 5 are to be expected. The anomalous asymmetry between cooling and heating (Fig. 6) is explained by the asymmetry between compression and tension in the stress versus time curve [Fig. 7(a)], which is reversed during heating. Details may be found in Ref. 36.

However, when the heating (cooling) process is complete, mechanical equilibrium is reached again. Hence, the system is allowed to remain at $P=0$ for a long time (or at a small pressure value due to the external perturbation that tracks the resonance frequency). As a consequence, all the units that changed state are subject to relaxation due to thermally activated random transition [note from Fig. 7(b) that for all them $P_2<0<P_1$]. To follow the recovery, in Fig. 7(c) we plot the quantity $\Delta N=N_2-N_1$, where N_2 and N_1 are the number of units that, at each time t, have changed their state during the process (i.e., from the state at $t=0$), switching to a rigid or elastic state, respectively. As observed, as soon as the temperature changes (at $t=0.4$ h), a net increase of soft units is created, which gradually relax back to a zero mean value, corresponding to a state, different, but equivalent, to the one at $t=0$. The relaxation data do not show a smooth recovery due to the limited number of units ($N=1000$) used in the simulations.

The PM distribution corresponding to the equilibrium state (just before t_c in Fig. 3) is reported in Fig. 7(d). Albeit

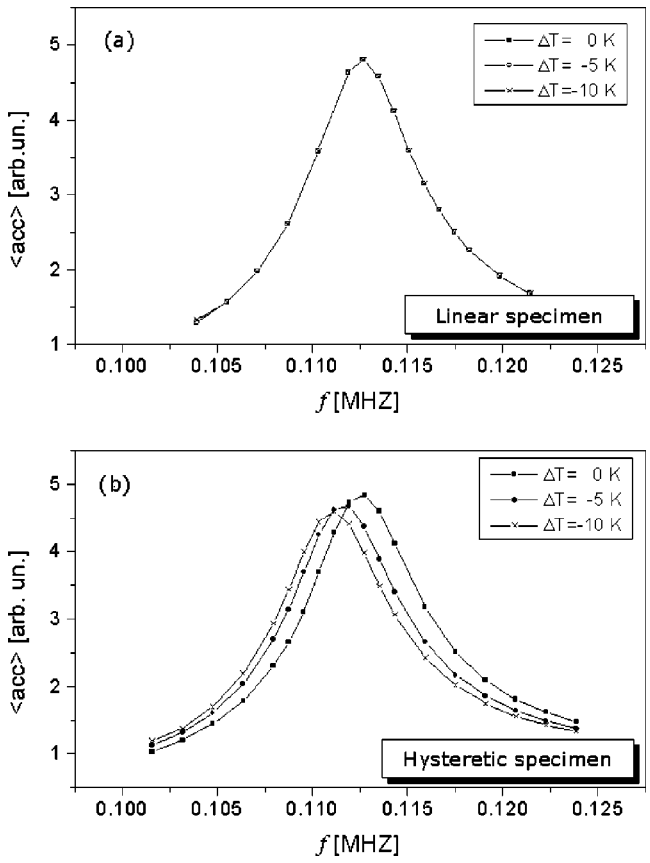

FIG. 8. Experiment type B: averaged acceleration vs frequency for different values of the external temperature shock. (a) linear specimen; (b) hysteretic specimen.

there are several differences from the $t=0$ state, the two are almost equivalent, as shown by the approximately same number of circles and triangles, which average to zero. It is to be noted that, at this stage, albeit the material is mechanically equivalent to that at the larger temperature, the net effect of the change in T_{ext} on the elastic properties of the grain remains and the resonance frequency is almost the same as if the material was linear. Again, results of Fig. 6 are justified.

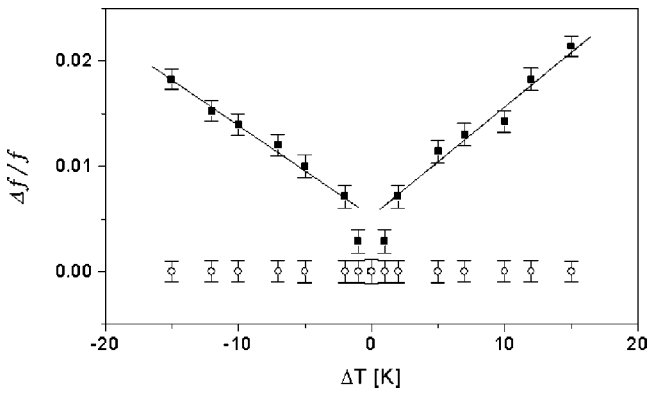

FIG. 9. Relative resonance frequency variation vs the temperature shock ΔT. Note that $\Delta T>0$ (<0) corresponds to heating (cooling).

C. Conditioning and relaxation due to thermally induced strains (experiment B)

Complementary results are obtained when a type B experiment is performed (see Fig. 3). A bar of hysteretic material is kept at room temperature and the resonance frequency is tracked (time t_a). Then a sudden change of the external temperature is applied and, after a short time and without letting the system relax, T_{ext} is brought back to room temperature. Then, f_r is measured again (time t_b) and, eventually, tracked with time (up to equilibrium at time t_c). The amount of thermal shock is quantified by the temperature change ΔT.

1. Conditioning effects

In Fig. 8, the averaged acceleration is plotted versus frequency for different ΔT, as reported in the plot, for both a linear [Fig. 8(a)] and a hysteretic [Fig. 8(b)] specimen. As expected, in the linear case the resonance frequency and specimen attenuation are unchanged after the thermal shock. In the case of a hysteretic material [Fig. 8(b)], the stress induced by the temperature change causes a softening (as discussed in the preceding subsection), which relax only very slowly with time (and in any case on a much longer time scale than the one needed to reach again thermal equilibrium at room temperature). Hence, the resonance frequency f_r drops down, with a shift increasing with ΔT.

In Fig. 9, the resonance frequency shift (percent variation of the resonance frequency after the thermal shock) is reported versus ΔT for both the linear (circles) and hysteretic (squares) case. It is noticeable the symmetry of the curve around $\Delta T=0$. As observed in experiments, the resonance frequency always decreases and the effect is ''almost'' independent of the sign (cooling or heating) of the thermal shock, provided its intensity is the same.

Finally, in Fig. 10 we explore the dependence of the softening effect on the external excitation amplitude. (Note that in Figs. 10 and 11, we have used a pressure interval $[-0.55, 0.55]$ MPa for the P_1 and P_2 range). In the first row of Fig. 10 the averaged acceleration is plotted versus frequency for different excitation amplitudes in the three columns. As visible by comparing the three plots, the resonance frequency before the shock, i.e., at $t=t_a$ (solid line), drops with the external amplitude: from $f_r\sim 0.113$ MHz at $F_0=0.006$ N up to $f_r\sim 0.111$ MHz at $F_0=0.16$ N. In contrast, the softening effect and increase of nonlinear attenuation due to the thermal shock (i.e., the difference between the sweeps at t_a and t_b, solid and dashed lines, respectively) is less and less evident with increasing the forcing, up to almost disappearing at $F_0=0.16$ N.

Such an effect can be understood by examining the distribution of interstices after the frequency sweep at $t=t_a$ (i.e., consequent to mechanically induced stresses due to the wave dynamics) and after the thermal shock at $t=t_b$ (i.e., consequent to a thermally induced stress), which are reported in the second and third rows for the three cases, respectively. (Again, circles denote interstices switched from the rigid to the elastic state, triangles vice versa, and dots units that have not changed their state.) A conditioning of the specimen is

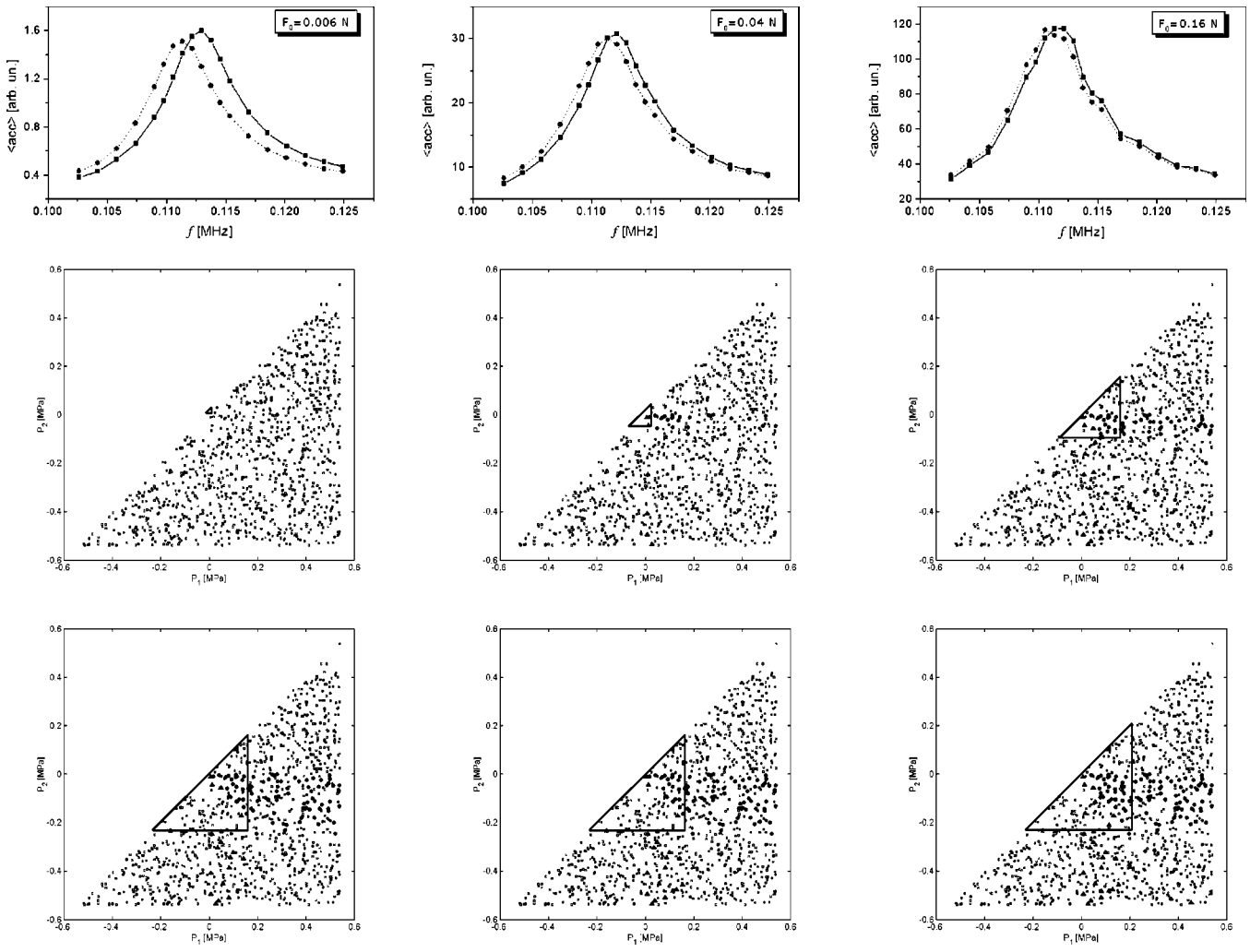

FIG. 10. Experiment B: determination of the resonance frequency for different values of the forcing amplitude after a cooling shock. First row: Averaged acceleration vs frequency before (solid line) and after (dotted line) the cooling shock. Second row: Corresponding distributions in the PM space after the sweep at room temperature before the shock ($T=300$ K), i.e., activation triangle for mechanically induced stresses. Small dots denote units that have not changed state from the initial one, triangles represent units shifted from the elatic to the rigid state, and circles denote units shifted from the rigid to the elastic state. The triangle marked in bold lines identifies the region swept by the acoustic standing wave in resonance. Third row: Corresponding distributions in the PM space after the cooling shock, i.e., activation triangle for thermally induced stresses. The triangle marked through bold lines identifies the region swept by the stress induced by the temperature change.

already visible after the first frequency sweep (second row), where for increasing F_0 the number of interstices that change state increases: the area in the PM space affected by the stress (called the ''activation'' area and represented by a triangle that corresponds to the applied pressure range) becomes larger. Such a conditioning results in a material softening with increasing the driving amplitude (more details can be found in Ref. 20). For the two lower amplitudes, the thermal shock causes a stress in the material larger than that due to the external perturbation. In fact, the variations in the PM space (third row) show an ''activation'' area much larger than the corresponding one in the second row. Hence, the state of the material before the second sweep is completely determined by the temperature variation. In fact, for both $F_0=0.006$ N and $F_0=0.04$ N the resonance frequency at $t=t_b$ is $f_r\sim 0.111$ MHz. In contrast, for $F_0=0.16$ N, the stress due to the external perturbation is close to that due to the temperature change. Hence the state before the second sweep is completely determined by a thermally induced conditioning of the same order of magnitude as the mechanical conditioning, which would have resulted from the first sweep and, therefore, the resonance frequency does not change. Such behavior cannot be easily experimentally observed, since the probing amplitudes are usually kept at very low levels.

The results previously described are resumed in Fig. 11, where the relative resonance frequency shifts are reported versus the excitation amplitude:

(a) In Fig. 11(a), the relative frequency variation δf_1 at $t=t_a$ (i.e., the percent change, when no thermal shock is

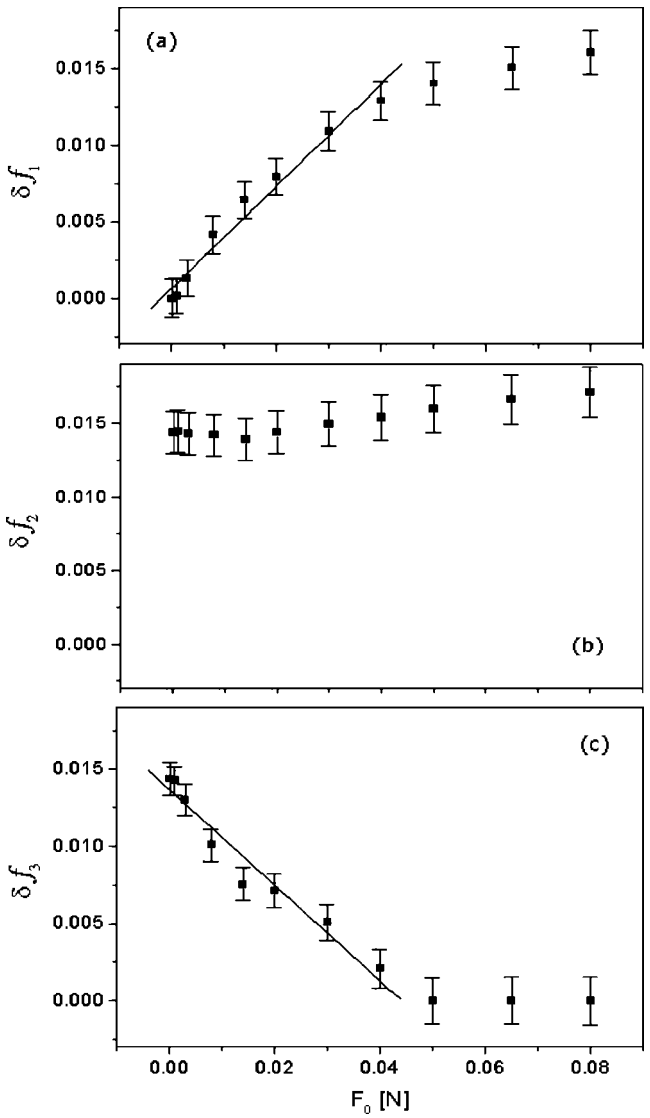

FIG. 11. Relative frequency shift vs the external forcing amplitude. (a) For each forcing the resonance frequency is measured at room temperature and the shift is calculated with respect to the linear (i.e., in the limit $F_0 \to 0$) limit (see text). (b) For each forcing the resonance frequency is measured at room temperature after the thermal shock and the shift is calculated with respect to the linear (i.e., in the limit $F_0 \to 0$) limit (see text). (c) For each forcing the resonance frequency is measured at room temperature after the thermal shock and the shift is calculated, for each F_0, with respect to the resonance frequency at the same forcing but before the shock (see text).

applied, of the resonance frequency at a given amplitude F_0 with respect to the resonance frequency at zero amplitude), defined as

$$\delta f_1 = \frac{\lim_{F_0 \to 0} f_r(F_0, t=t_a) - f_r(F_0, t=t_a)}{\lim_{F_0 \to 0} f_r(F_0, t=t_0)},$$

is reported versus F_0. In agreement with experiments, the frequency shift (of the order of a few percent) is linear (at low forcing) with the external driving amplitude. For larger forcing, as also observed experimentally, saturation occurs. In our simulations, such an effect corresponds to a saturation in the PM space distribution (the expected stress for $F_0 = 0.32$ N is about 0.36 MPa).

(b) In Fig. 11(b), the relative frequency variation δf_2, defined as in the previous case, but considering a sweep over amplitude after the thermal shock,

$$\delta f_2 = \frac{\lim_{F_0 \to 0} f_r(F_0, t=t_a) - f_r(F_0, t=t_b)}{\lim_{F_0 \to 0} f_r(F_0, t=t_a)},$$

is reported versus F_0. As expected, the resonance frequency is no longer amplitude dependent, as the conditioning due to the thermal shock is much larger than that caused by the wave dynamics. A slight dependence is observed, as expected, only for large forcing.

(c) In Fig. 11(c), the relative frequency variation δf_3 (i.e., the percent change, for each amplitude, of the resonant frequency after the thermal shock with respect to the resonance frequency at the same amplitude before the thermal shock), defined as

$$\delta f_3 = \frac{f_r(F_0, t=t_a) - f_r(F_0, t=t_b)}{f_r(F_0, t=t_a)}$$

is reported versus F_0. As expected from the previous discussion, the change in resonance frequency almost disappears for large driving amplitudes (from 1.6% at the lower amplitude). The relative frequency variation seems to decrease linearly with F_0 for low values of excitation.

D. Recovery and slow dynamics after thermal shock

As a last experiment, in Figs. 12 and 13 we consider examples of the recovery of the elastic properties after softening due to a thermal shock, i.e., we consider experiment B from time t_b to t_c. In Fig. 12(a), the resonance frequency is plotted versus time for different values of the transition probabilities q_1 and q_2 as reported in the figure. Note that the ratio $q_2/q_1 = 0.03$ is kept constant to ensure that the three cases have the same equilibrium condition at zero pressure (i.e., the same initial state), as shown by the fact that the resonance frequency before the thermal shock does not depend on the rates. Immediately after the thermal shock ($\Delta T = -20$ K), frequency drops down, as already discussed in the preceding subsection. Later, it slowly recovers the original value. Of course, larger rates produce a faster recovery.

The most striking feature of such a recovery, similar to the one already presented in Fig. 6, is that, for a large time interval, f_r grows logarithmically with time. Such a $\log_{10}(t)$ behavior, which has been always observed for any kind of recovery in hysteretic media, is more evident in Fig. 12(b), where the same plot as in Fig. 12(a) is reported, but in a semilogarithmic scale. The solid line represents a fit of the form

$$f_r = A + B \log_{10}(t - t_0). \tag{13}$$

The fitting gives a correlation coefficient larger than 0.99 for the three cases. The parameter A is the same ($=0.11$ MHz) for the three curves, corresponding to the frequency drop immediately after the shock, while B increases with increas-

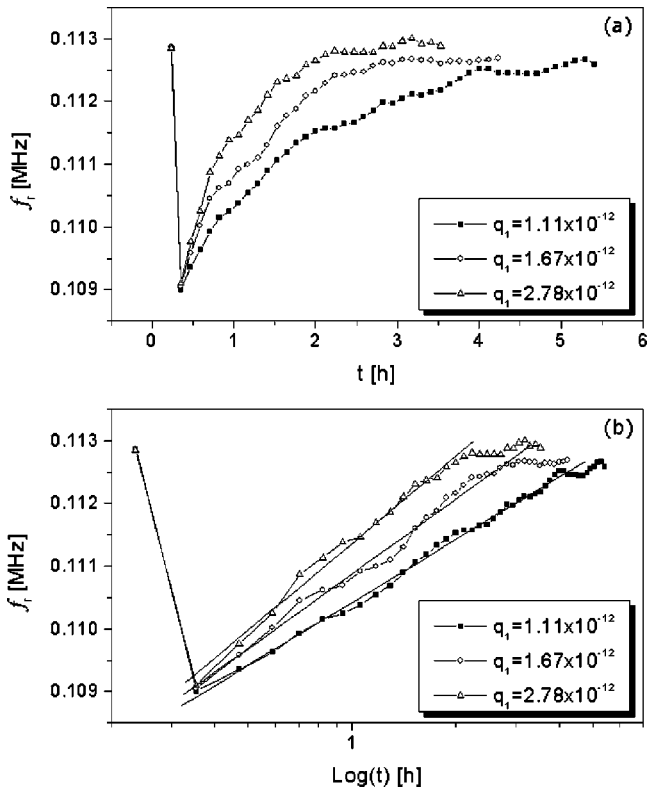

FIG. 12. Recovery after thermal shock: resonance frequency (a) vs time or (b) vs $\log_{10}$ (time) for different relaxation rates. $q_2 = 0.03q_1$ always.

ing q_1 ($B = 0.33\times10^{-2}$, 0.40×10^{-2}, 0.45×10^{-2} MHz), and t_0 is the time at which the thermal shock occurs.

In Fig. 13, we simulate a recovery after thermal shocks of different intensities (increasing ΔT as reported in the figure). The resonance frequency is reported versus time in a semilogarithmic plot, to show the $\log_{10}$ (time) behavior in the recovery phase. Solid lines represent fitting in the form of Eq. (13). It is noticeable that both A and B depend on ΔT, i.e., both the frequency drop and the slope of the recovery curve increase with increasing ΔT. As a result, the time at which recovery can be assumed as completed (time t_c in Fig. 3) is approximately the same for the considered cases. The near

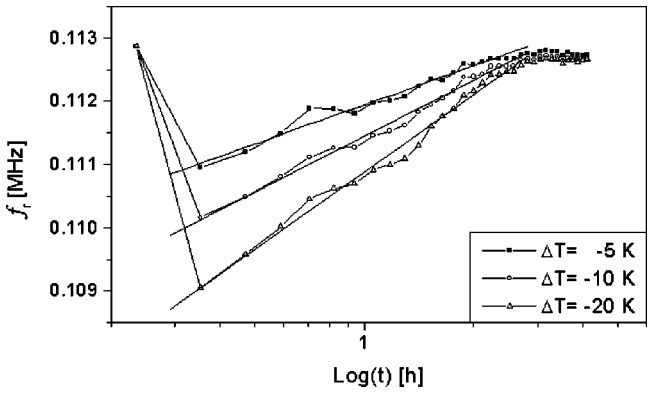

FIG. 13. Recovery after thermal shock: resonance frequency vs $\log_{10}$ (time) for different thermal shock amplitudes.

independence of the recovery time from the shock amplitude has been observed experimentally in the case of mechanical stresses (see Fig. 5 of Ref. 7).

IV. DISCUSSIONS AND CONCLUSIONS

In this paper we have shown that the anomalous elastic behavior experimentally observed for rocks and other mesoscopic materials can be explained in terms of a balance between the ''normal'' dependence of the elastic constants on temperature[28] and the nonlinear softening caused by thermally induced stresses. The former predicts softening (hardening) depending on the sign of temperature variation, heating (cooling), while the latter always predicts softening. In fact, thermal shocks (or temperature variations) cause deformations, hence stresses, in the material and, as shown both experimentally[7,26] and theoretically,[20] the softening does not depend on the sign of the stress.

To support our claim, we have extended, by introducing only well-known linear thermoelastic equations,[27] a model previously developed[19,20] that has proven to describe well the phenomenology due to mechanical stresses, by considering thermal random transitions between two different states (which are not related to any external temperature variation). The resulting model has been capable of reproducing qualitatively the available experimental data, including both resonance frequency variations, conditioning, and slow dynamics. It is to be noted, however, that such anomalous elastic effects, appearing as a consequence of thermal changes, are only indirectly related to the temperature variation through thermal expansion.

In this paper, we have also presented an analysis of the role of some of the parameters. Our simulations may suggest new experiments to be performed in order to add information about the phenomenon and further validate or reject our model. Among them, the claim that the effect becomes less and less evident with increasing the forcing amplitude (see Fig. 11).

Additional interesting features have not been explored here, due to lack of space, but are intrinsic to the model. Some of them will be discussed elsewhere, such as the explanation for the larger frequency drop when the specimen is cooled rather than heated[36] and the complex variety of behaviors that can be obtained when varying parameters. For example, Lavoux limestone might present particularly interesting features, since it presents a ''hardening when heating'' relation [opposite to Eq. (3)]. Particularly interesting will be the tracking of the resonance frequency when the temperature is continuously varied with time. In such a case, a hysteretic like behavior when the system is subject to a cyclic temperature protocol is expected.

In conclusion, we emphasize that the model presented here, albeit capable of reproducing well the observations we are aware of, should be modified to include more realistic or physical features. For example, the probabilities for the random transitions between states must be temperature dependent (and perhaps also pressure dependent). More important, the hypotheses of the instantaneous reach of thermal equilibrium within the interstice must be substituted by a reasonable model. Such improvements will surely help in catching de-

tails that the present model does not allow us to see and perhaps will suggest a physical comprehension of the mechanisms involved. However, we believe that the philosophy of our approach and the claims for the explanation will not be modified.

ACKNOWLEDGMENTS

The work was supported by MURST (Grant No. MM02328989). The authors also acknowledge the support of the European Science Foundation (NATEMIS Programme).

*Email address: m_nobili@libero.it
†Email address: marco.scalerandi@infm.polito.it

[1] R. A. Guyer and P. A. Johnson, Phys. Today **52** (4), 30 (1999).
[2] R. A. Guyer, K. R. McCall, and G. N. Boitnott, Phys. Rev. Lett. **74**, 3491 (1995).
[3] R. A. Guyer, J. A. Tencate, and P. A. Johnson, Phys. Rev. Lett. **82**, 3280 (1999).
[4] V. Zaitsev, V. Gusev, and B. Castagnede, Ultrasonics **40**, 627 (2002).
[5] J. A. TenCate, K. E.-A. VanDenAbeele, T. J. Shankland, and P. A. Johnson, J. Acoust. Soc. Am. **99**, 3334 (1996).
[6] J. A. TenCate and T. J. Shankland, Geophys. Res. Lett. **23**, 3019 (1996).
[7] J. A. TenCate, E. Smith, and R. A. Guyer, Phys. Rev. Lett. **85**, 1020 (2000).
[8] F. Cleri, S. Yip, D. Wolf, and S. R. Phillpot, Phys. Rev. Lett. **79**, 1309 (1999).
[9] I. Y. Smolin, P. V. Makarov, D. V. Shmick, and I. V. Savlevich, Comput. Mater. Sci. **19**, 133 (2000).
[10] See, for example, V. Zaitsev, V. Gusev, and B. Castagnede, Phys. Rev. Lett. **89**, 105502 (2002).
[11] D. J. Holcomb, J. Geophys. Res. **86**, 6235 (1981).
[12] K. R. McCall and R. A. Guyer, Non Linear Processes in Geophysics **3**, 89 (1996).
[13] K. E.-A. VanDenAbeele, P. A. Johnson, R. A. Guyer, and K. R. McCall, J. Acoust. Soc. Am. **101**, 1885 (1997).
[14] B. Capogrosso-Sansone and R. A. Guyer, Phys. Rev. B **66**, 224101 (2002).
[15] R. S. Schechter, H. H. Chaskelis, R. B. Mignogna, and P. P. Delsanto, Science **265**, 1188 (1994); P. P. Delsanto, R. Mignogna, M. Scalerandi, and R. Schechter, in *New Perspectives on Problems in Classical and Quantum Physics*, edited by P. P. Delsanto and A. W. Saenz (Gordon and Breach, New Delhi, 1998), Vol. 2, pp. 51–74.
[16] P. P. Delsanto and M. Scalerandi, J. Acoust. Soc. Am. **104**, 2584 (1998).
[17] E. Ruffino and M. Scalerandi, Nuovo Cimento Soc. Ital. Fis., B **115**, 645 (2000).
[18] M. Scalerandi, P. P. Delsanto, and P. A. Johnson, J. Phys. D **36**, 288 (2003).
[19] V. Agostini, P. P. Delsanto, P. A. Johnson, and M. Scalerandi, J. Acoust. Soc. Am. **113**, 3049 (2003).
[20] P. P. Delsanto and M. Scalerandi, Phys. Rev. B **68**, 064107 (2003).
[21] K. van den Abeele, P. A. Johnson, and A. Sutin, Res. Nondestruct. Eval. **12**, 17 (2000).
[22] B. Zinszner, P. A. Johnson, and P. N. J. Rasolofosaon, J. Geophys. Res. **102**, 8105 (1997).
[23] K. van den Abeele, J. Carmeliet, P. A. Johnson, and B. Zinszner, J. Geophys. Res. **107** (B6), ECV4-1-11 (2002).
[24] T. J. Ulrich and T. W. Darling, Geophys. Res. Lett. **28**, 2293 (2001).
[25] Results presented at the International Workshop on Nonlinear Elasticity in Materials, July 2003, Santa Fe, NM (unpublished).
[26] See, for example, R. Guyer and P. A. Johnson, J. Mater. Process. Manuf. Sci. **9**, 14 (2000).
[27] L. D. Landau and E. M. Lifshitz, *Theory of Elasticity* (Pergamon, Oxford, 1986).
[28] Y. P. Varshni, Phys. Rev. B **2**, 3952 (1970).
[29] G. Gremaud and S. Kustov, Phys. Rev. B **60**, 9353 (1999); E. Nadgornyi, Prog. Mater. Sci. **31**, 210 (1988); J. Baur and W. Benoit, J. Appl. Phys. **60**, 3473 (1986).
[30] A. Aknine, B. Castagnede, and C. Depollier, C. R. Acad. Sci., Ser. IIb: Mec., Phys., Chim., Astron. **324**, 501 (1997); R. Steck, P. Niederer, and M. L. Knothe-Tate, Med. Eng. Phys. **22**, 117 (2000).
[31] X. Xia and P. G. Wolynes, Phys. Rev. Lett. **86**, 5526 (2001); V. Lunchenko and P. G. Woylnes, *ibid.* **87**, 195901 (2001).
[32] K. van den Abeele, J. Acoust. Soc. Am. **99**, 3334 (1999).
[33] J. A. Tencate (private communication).
[34] See H. F. Pollard, *Sound Waves in Solids* (Methuen, New York, 1977), p. 107.
[35] M. Nobili and M. Scalerandi (unpublished).
[36] P. P. Delsanto, M. Nobili, and M. Scalerandi, Physica Scripta, Proceedings of the I European Conference on Applied Physics, Badajotz, October 2003, in press.